UNIVERSITY OF TWENTE.

Department of Biomedical Signals and Systems (BSS)

Acquiring Head Orientation through using an IMU with Madgwick Orientation Filtering

Pim Jansen

B.Sc. Thesis
March 2024

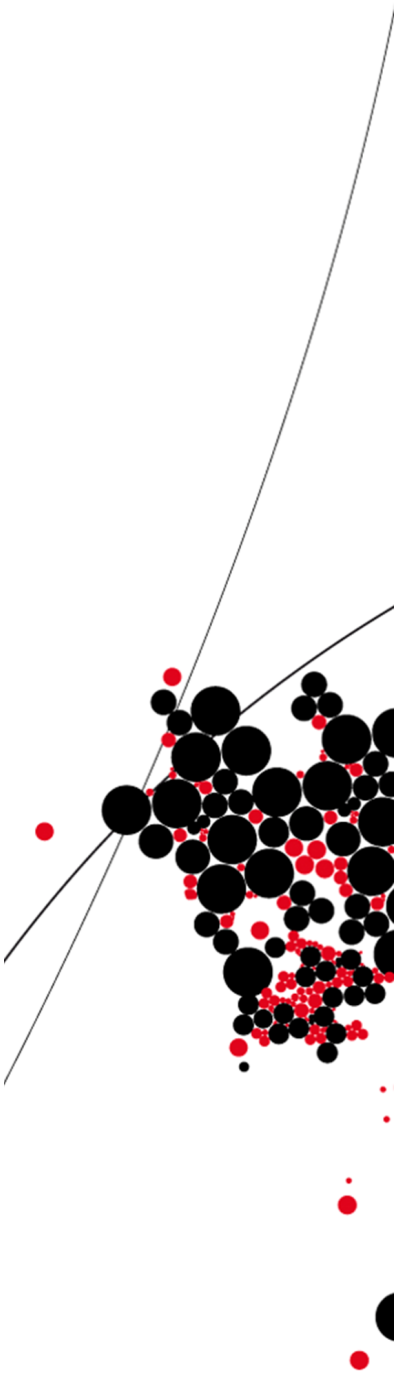

Examination committee:
dr. ir. B.J.F. van Beijnum.
Msc. S.J. Mevissen
dr. ir. M.I. Refai

Department of Biomedical Signals and Systems
University of Twente
P.O. Box 217
7500 AE Enschede
The Netherlands

1 Abstract

DMEK (Descemets' Membrane Endo Keratoplasty) corneal transplantation is an eye surgery in which the head orientation plays an important role in the occurrence of graft detachment. The patient is instructed to stay in the supine position and look up for 24 hours post-surgery. In some cases, however, graft detachment occurs which leads to an additional intervention. In this research, the focus is on obtaining the orientation of the head by applying the Madgwick orientation filter to an IMU attached to the patient's forehead.

Accordingly to this problem, the purpose of this research part is to optimise the filter parameter β and apply sector division on head poses. Optimising this filter parameter enhances the orientation estimation.

The outcomes of the study revealed the significance of optimizing the filter parameter β to enhance head orientation determination. The implementation of sector division for head poses further contributed to understanding the patient's postoperative behaviour. This groundwork holds promise for improving patient care outcomes in corneal transplantation, ultimately reducing the incidence of graft detachment and the need for additional interventions.

Contents

2 Introduction

In 2018, approximately 1700 corneal transplantations were performed in The Netherlands and this number is even increased in recent years [1]. This research focuses specifically on the Descemet's Membrane Endothelial Keratoplasty (DMEK) corneal transplantation. A DMEK surgery is needed when the inner cell layer of the cornea (as can be seen in figure 1) stops working properly. This can be due to Fuchs' dystrophy [2], bullous keratopathy, iridocorneal endothelial (ICE) syndrome, or other endothelial disorders. In this surgery, the recipients' Descemet's membrane and endothelium are selectively removed and replaced by transplantation of a donor Descemet's membrane and corneal endothelium. This is performed specifically without additional donor stromal tissue [3].

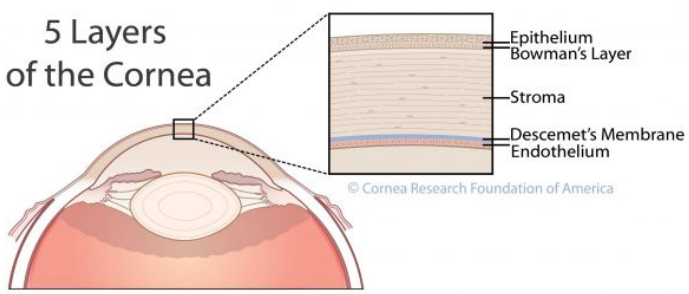

Figure 1: *Anatomy of the 5 layers of the human eye. As can be interpreted, Descemet's membrane is one of the inner layers of the eye [4].*

The surgery is carried out with the help of an air bubble to keep the new cell layer in place. Sometimes, however, the graft becomes detached and needs to be re-inflated. This "re-inflation" means that an air bubble will be applied again. At this point, the protocol states that the patient is instructed to stay in the supine position(lie flat on their back and looking up) for 24 hours after surgery. The reason for keeping this position is that air rises, which in this case presses the donor graft to the cornea, thus improving graft fixation. Lying flat and looking up for 24 hours is difficult, especially for elderly patients. For a human, it is difficult to keep his or her head in a constant position for a long period (e.g. 24 hours), because the urge to move the head is strong and accidental movement may occur. The overall study is about the relation between graft detachment and maintaining supine positioning. In short, is it really necessary to lie flat and look up for 24 hours to prevent graft detachment? If not, different scenarios are possible. Firstly, the current post-surgery protocol should not be used anymore. Secondly, the outcome of the research can lead to a different posture being most optimal to prevent graft detachment.

The orientation of the head plays an important role in this research, as graft detachment could occur when the head is moving and so are the eyes. At the moment, the interpretation of the data is unclear because there is still no way of obtaining the orientation of the head. The goal of this part of the research is specifically obtaining the orientation of the head, with an orientation filter called Madgwick filter. A part of the goal contains parameter optimization for optimal orientation and finally sectors of head poses are defined based on the obtained head orientations. These head pose sectors contributes to the overall research as they can be applied to patient data. The ideal outcome would be that the different head pose sectors are well defined so that percentages of occupation of the poses can be linked to the patient data.

To acquire this orientation, an IMU (Inertial Measurement Unit) sensor is used. Using an orientation filter

(Madgwick) and this sensor, the orientation of the head concerning an initial body frame can be determined. This orientation filter fuses the data received from the IMU to provide it in an interpretable form.

3 Theoretical aspects

3.1 Inertial Measurement Unit (IMU)

The sensor used is an IMU (Inertial Measurement Unit). It is a device that combines different sensors to measure, with which motion and orientation in space can be obtained. It contains an accelerometer, which measures linear acceleration along the device's axes. Thereby it contains a gyroscope, which measures the rate of rotation around the axes, also called the angular rate. Finally, it measures the magnetic field surrounding the system, with the magnetometer.

This is all to obtain the orientation of the sensor. Each of these contains 3 axes, which makes in total of 9 axes. In this project a 6-axis IMU, the "Axivity AX6" has been used, shown in figure 2. This means that the IMU in this research just contains and uses accelerometer and gyroscope data.

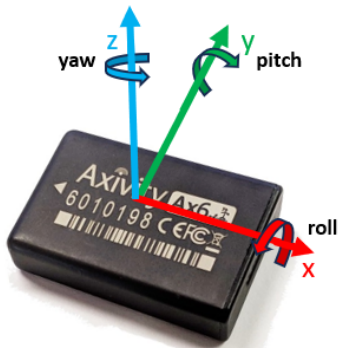

Figure 2: *Illustration of the IMU used. Orientation around the axes, containing three degrees of freedom (roll (x), pitch (y) and yaw (z)).*

3.1.1 Orientation field (XYZ)

As mentioned in 3.1, the sensor does not contain a magnetometer, which for the orientation means that a relative measurement orientation is used instead of absolute. Measurement orientations which are absolute use a magnetic field to orient itself, whereas relative measurement orientations are relative to the orientation the IMU has at the moment the measurement started [5].

In order to describe the orientation field, figure 2 is used. This IMU is free to rotate in three dimensions. Firstly, the roll is a rotation over the length of the IMU. Thereby, the pitch rotation is a rotation over the width of the IMU. The third dimension is the rotation around its axis, the yaw. Respectively these are rotations around the x, y and z axis, which are called the Euler angles, further explained in section 3.3.3.

3.2 Madgwick Orientation filter

A suitable filter for integrating the data from both the accelerometer and gyroscope is the Madgwick filter, developed by Sebastian Madgwick. This filter effectively tracks orientations by leveraging the data provided by both sensors [6].

The Madgwick orientation filter's task is to compute estimates of orientation through the optimal fusion of these gyroscope and accelerometer measurements [6]. An overview of the steps the filter conducts are shown in figure 3. The overview describes the steps made in the Madgwick algorithm starting with the gyroscope and accelerometer data and ending with the estimated orientation. A more specific overview of the Madgwick filter derivation is described in Madgwick's paper [6]. What makes the Madgwick filter different from other orientation filters is that it can operate at low sampling rates and has adjustable parameters. Being able to perform at low sampling rates reduces the hardware and power required for wearable inertial motion tracking, enabling low-cost systems that can operate for extended periods of time [7]. In addition, the Madgwick filter is able to compensate for gyroscope bias drift over time [6].

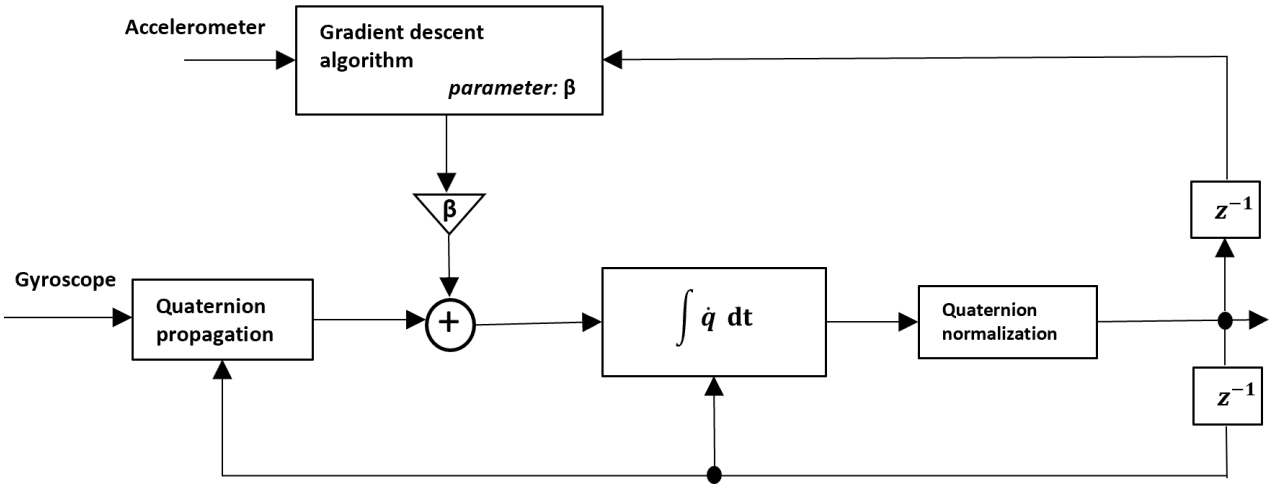

Figure 3: *Block diagram which gives an overview of the steps made to obtain the orientation [8]. The gradient descent corrective step is combined with the gyroscope data from the $\dot{q}$, which will be integrated with the sampling rate. Consequently, the obtained quaternions are normalized. This results in the estimated orientation.*

With this Madgwick filter the orientation can be obtained. There are several ways to represent and orient the Madgwick-filtered data. These are quaternions, rotation matrices and Euler angles. Each of them respectively explained in 3.3.1, 3.3.2 and 3.3.3.

In this study, an existing algorithm developed by Sebastian Madgwick was utilized [6]. Madgwick's algorithm involves multiple steps to determine orientation, as outlined in Figure 3. One of these steps employs the gradient descent algorithm, an optimization technique that utilizes accelerometer readings to estimate local gravity [9]. Meanwhile, gyroscope data is used for estimating attitude through numerical integration.

3.2.1 Parameters

There is only one parameter in the Madgwick filter which can be adjusted, a filter gain indicated as β. This β is a tradeoff between the gyroscope and accelerometer, further explained in this section.

The β filter gain represents the mean zero GME (Gyroscope Measurement Error), the magnitude of a quaternion derivative. These errors can be caused by sensor noise, calibration errors, sensor miss-alignment and more [6].

Equations 1 and 2 show how this filter gain, β is calculated [6]. Equation 1 describes the degrees to radians conversion and equation 2 computes the β. To be able to calculate this filter gain, the GME of the IMU used should be known. This GME value can be found at the specifications of the Axivity AX6, written down in 4.1. Using the formulas and following the specifications, a default value of $\beta = 0.045$ results.

$$gyroMeasError = \pi * (GME/180.0) \tag{1}$$

$$\beta = \sqrt{3/4} * gyroMeasError \tag{2}$$

Important to know is that the β is not already the optimized value. The β gain needs to be finetuned by performing experiments until a satisfactory result is reached. Finetuning this parameter leads to higher accuracy of the orientation positions

The filter parameter (β) in the Madgwick filter is a tradeoff between accuracy and response speed. Prioritization of the gyroscope and accelerometer are playing a key role in this tradeoff. A low filter gain indicates dominant gyroscope influence and a high filter gain value indicates accelerometer dominance.

3.2.2 Drift Minimization

Following the literature, orientation drift will occur over a long observation interval. This is mainly caused by the time integration of the angular velocity, where non-stationary bias is corrupting this integration [10]. Non-stationary bias is a situation in which the properties of a system change over time [11]. The accelerometer can compensate for this gyroscope drift.

3.3 Visual Representation

In order to acquire a visual representation of Madgwick's filter output, there are multiple manners to visualize the obtained orientations. These are all described in sections 3.3.1, 3.3.2 and 3.3.3 below.

3.3.1 Quaternions

The Madgwick filter formulates the attitude estimation in the quaternion space. The rotation quaternions are a mechanism for representing rotation in three dimensions. These three dimensions are expressed with four-dimensional numbers of the form $w+xi+yj+zk$, where the coefficients w, x, y, z are real numbers and $1, i, j, k$ are the basic vectors [12]. The quaternions are difficult to interpret for humans, so other methods are used to obtain a well-interpreted way. Furthermore, the dimension of the representation of a rotation as a quaternion is 4 numbers. This relatively small size results in faster multiplications.

3.3.2 Rotation Matrix

Another type of representation is with rotation matrices. These matrices can be used to represent rotations in Euclidean space and are widely used for calculations in geometry. Rotation matrices are obtained from quaternions and can be defined for 3-dimensional spaces and are always 3×3 matrices. For the representation as a rotation matrix, there are 9 numbers used [13].

3.3.3 Euler Angles

In order to get a view as a human on the orientation of the angles created, Euler angles are used. These Euler angles are introduced to describe the orientation of a rigid body concerning a fixed coordinate system [14]. As mentioned earlier in section3.1.1, the Euler angles are represented as roll, pitch and yaw (respectively x, y and z) in the Cartesian coordinates system.

Gimbal lock is a mathematical problem, which occurs only when Euler angles are used in the computations or are used to represent 3D orientation. It occurs when two of the three axes of rotation of a 3D object align,

which results in a loss of one degree of freedom as can be seen in figure 4 [15][16]. These Euler angles are useful to get an idea of the orientation, as they can be interpreted well. But to avoid Gimbal lock in the visualisation, it is necessary to use quaternions or rotation matrices instead of Euler angles.

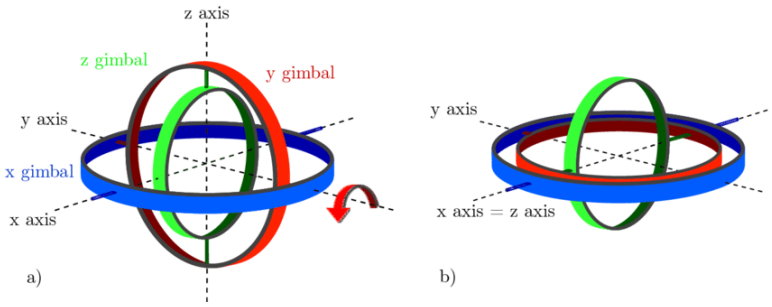

Figure 4: *Gimbal lock principle. As can be seen, when two of the three axes of the rotation align with each other, gimbal lock occurs [16].*

3.4 Head Poses

As mentioned in the introduction, head poses will be defined from the orientation obtained. The head pose refers to the view of the face at a certain angle. There are two different typical movements of the head, the in-plane (z) and out-of-plane (x,y) movement [17]. The in-plane movement is observed when the face is rotating along the axis of the face [18]. As can be seen in figure 5, the human head has 3 degrees of freedom (DOF). These are the possible rotations around the three different axes as already mentioned in 3.3.3.

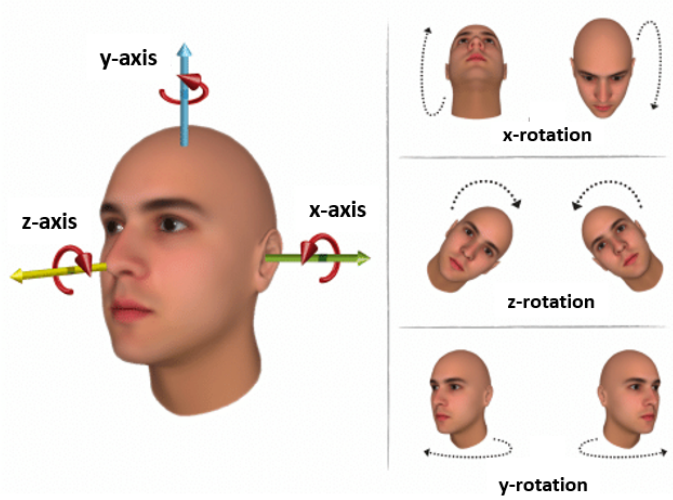

Figure 5: *Orientation of the head defined in terms of x-, y- and z-rotations describing the three degrees of freedom of the human head [19].*

These defined head poses can make the step between the Madgwick's filter obtained orientation and the DMEK case. This is through defining sectors of how much of the time the head is posed at a certain angle (x, y, z). To translate this to the medical case: how much of the time the head is oriented in the right way? "Right way" means in this case looking straight up, since this is instructed to the patients that this is most optimal for preventing graft detachment. Since the z-rotation is an in-plane movement and makes no sense to the medical case, the head poses of x- and y-rotations are used.

3.5 Bed Calibration

Since there are multiple orientation frames, the global, sensor and segment frame. A sensor-to-segment calibration is performed to convert the data of the sensor to the segment's frame. The sensor-to-segment calibration is performed here as bed calibration by rotating the transversal axis while the patient is lying on a bed (shown in figure 6). This calibration is performed for the deviation created by an IMU which is not lying straight on the head. As a result of the bed calibration, the z vector is calibrated to [0 0 1]. After the bed calibration, a pachymetry scan is applied to measure the thickness of the cornea. Subsequently, the patient returns 24 hours post-surgery back to the hospital, where the sensor is removed from the patient's head. Since this bed calibration is performed, it can be assumed that the sensor-to-segment orientation is going well at the patient data

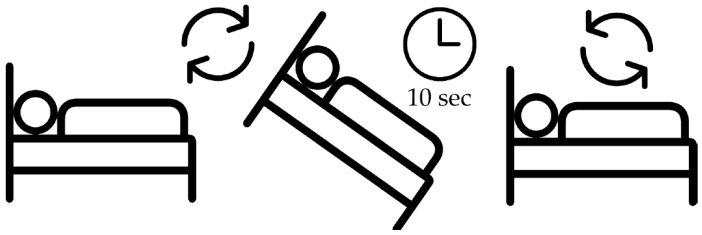

Figure 6: *Bed-calibration applied directly after the surgery by rotating the bed around the transversal axis for 10 seconds and back.*

4 Materials and Methods

4.1 Materials

Materials such as devices (specifications included) and programs which are used, described in table 1.

Material/Tool	**Specification**
Axivity AX6 IMU	Gyroscope Measurement Error: 3°/s Gyroscope Range: ±125/250/500/1000/2000 °/s Accelerometer Range: ±2/4/8/16 g
OmGui Open Movement	The OmGui Open Movement software, available on GitHub [20].
IMU patient data (24-hours data)	Data collected from patients using IMU sensor
Integrated Development Environment (IDE) "Spyder"	To apply the Madgwick filter and make visualizations (See Appendix A.1 for an algorithm pipeline)

Table 1: *Materials and Specifications*

4.2 IMU Positioning

In the patients' situation, the IMU is attached to the forehead with paper bandages, as shown in figure 7. For 24 hours postoperative where the patient is instructed to stay in supine position. Driving home and other obligations, however, are allowed. When the IMU is attached to the forehead, the orientations (x, y and z) of the head (figure 5) and the IMU (figure 2) are matching, for clarity.

The experiments involving validation and calibration are conducted using self-generated data and utilize an IMU attached to a rectangular object. This configuration facilitates precise angle measurements with the IMU.

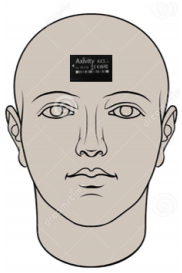

Figure 7: *IMU positioned on the patient's forehead.*

4.3 Data acquisition

An IMU is used to receive the data, as mentioned in 3.1. Described in table 1, the data is obtained using an application from Github called OmGUi Open Movement. Where the sampling frequency and gyro range are fixed. The values used are for the sampling frequency, gyro range and accelerometer range respectively 200 Hz, 1000 dps (degrees per second) and 8 g (standard gravity).

Several requirements were stated for DMEK patients to be able to participate in the project. At this moment data is collected from about ten participants. From these, data collections of two patients are used in this research.

4.4 Model Validation

In order to ensure that the system is valid, calibration and validation are applied to raw data.

4.4.1 Sensor Calibration

The first step is to maintain the IMU's angle accuracy, thus a calibration (another calibration than mentioned in 4.3) of the gyroscope has been performed [21]. This calibration includes creating rotations of the device for each Euler angle rotation (x, y, z). Subsequently, the data of the gyroscope is integrated over time, which results in the total angle, expressed in degrees (shown in table 3). Since a 360 °rotation is applied, the expected would be a total rotation of also 360 °. The deviations were negligible, thus data compensation was not needed.

The integration of gyroscope data to calculate accumulated angles over time can be represented by the following formula:

$$\sum_{i=1}^{n} \omega_i \cdot \Delta t = \theta_i \tag{3}$$

where:

- ω_i is the angular velocity at time step i,
- Δt is the time interval between data points,
- n is the total number of data points, and
- θ_i is the accumulated angle at time step i.

4.4.2 System Validation

Validation is applied to test the accuracy created by the calibration step. This validation is performed by attaching a protractor to the IMU. Measurements are performed with different rotations: 45, 90 and 180 degrees rotations, applying to each Euler angle (x, y, z). The validation has been performed with a form of Face Validity. Face Validity is a method which makes a direct assessment of how the measurement appears and if it is performing what is expected. In figure 8 (a) and (b), rotations of 45 and 90 degrees of the IMU are shown.

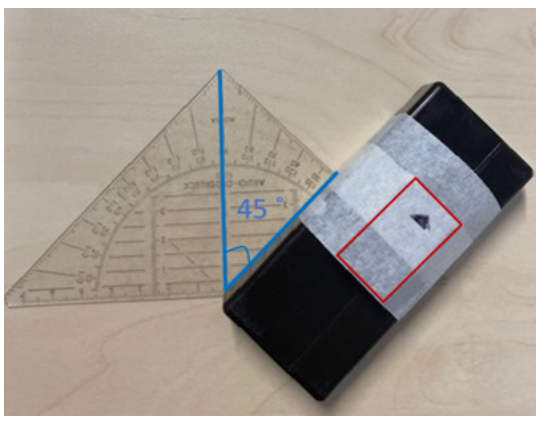

(a) 45 °

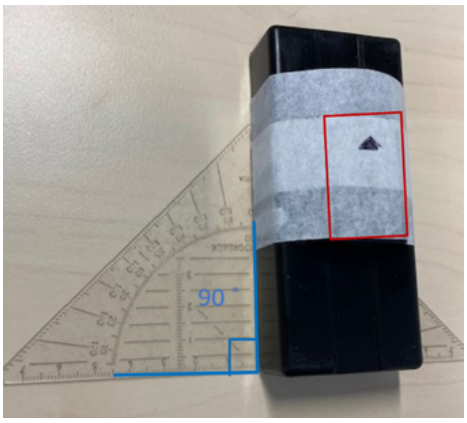

(b) 90 °

Figure 8: *Validation method at (a) 45 °and (b) 90 °. The red outlined rectangle indicates the placement of the IMU device on a rectangular object.*

4.5 Methods

The measurements performed are firstly, the filter has been used with small measurements. This is to check if it outputs expected values which is part of the validation. Secondly, measurements are performed for optimisation of the beta parameter. After that, the optimised filter was applied to patients' data, which were subsequently distributed and visualized in a circular plot. This is the main line of experiments performed.

First of all, the β parameter must be optimised to obtain measurements with the highest accuracy. Optimisation of this parameter in Madgwick's orientation filter is achieved by fine-tuning this beta value because the beta value is a tradeoff between the sensitiveness of the gyroscope versus the accelerometer (as mentioned in 3.2.1),

After that, small checks for determining sectors of the head pose areas are performed. This contains a sanity check which creates and controls measurements and after that, the patient's data is implemented in the head pose sectorplot.

4.5.1 Beta Parameter Optimisation

The experiment has been performed as follows: β gain values in a range of 0.01 till 0.5 are set to observe the influence of the β gain on measurements with velocity varying [6]. In this experiment, the default β value (β = 0.045, see section 3.2.1) is kept in mind .

The experiments imply 180 ° rotations on all three rotation axes (x,y and z). The duration of the measurements is in total 10 minutes consisting of $+180°$ rotations and back to the start position, ten times iterated. This

categorization is made to investigate the influence of the β parameter on the conversion of a constant velocity movement to a stationary period (no movement). The velocities are categorized into slow, medium and fast in table 2.

Category	Velocity (°/s)
Slow	18 °/ s
Medium	36 °/ s
Fast	72 °/ s

Table 2: *Quantification of the velocities, categorized into slow, medium and fast. The velocities are quantified based on one 180 °rotation.*

Subsequently, periods are selected by selecting the periods in which the IMU should be at the start position (angle = 0 °). For the 10 minute measurement this results in 10 stationary periods. This selection is based on the Euler angles as the rotation patterns are well visualised. In figure 9 a visualisation of how periods are selected is shown.

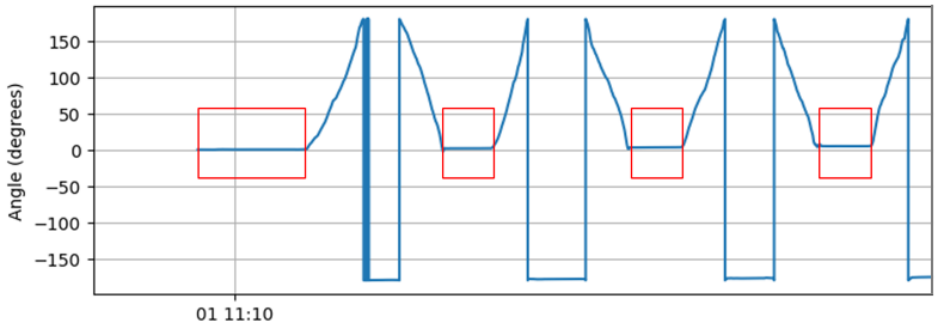

Figure 9: *Selection of the stationary periods, showed with the red brackets. The selection is performed in the Euler angle representation.*

To investigate the influence of the parameter on the stability of the movements the RMSE (Root Mean Square Error) measurement is performed on the rotation matrices [22]. It evaluates in this case the difference between what is measured (y_i) and the true value ($\hat{y}_i$) over an amount of datapoints (n) [23]. The true value obtained from the rotation matrix: the three vectors (x, y and z) at the stationary periods (angle = 0 °).

$$RMSE = \sqrt{\frac{1}{n}\sum_{i=1}^{n}(y_i - \hat{y}_i)^2} \tag{4}$$

Since the RMSE is calculated over stationary periods, the RMSE gives a picture of the influence of the parameter on the movements performed, with particular attention paid to performance in terms of accuracy. The predicted values are the start position values which can be seen as 3D identity matrix.

4.6 Head Pose Sectors

4.6.1 Projected Vectors

Returning to head poses, sectors are created to define these poses in areas (an example is shown in figure 11. Consequently, the sector plots are applied to the 24-hour patient data. Since these sectors are 2D whereas the vectors are 3D, a 3D to 2D conversion has been applied. The method used involves vectors projected ($\vec{v}_p$) onto a 2D plane, shown in equation 5:

$$\mathbf{v}_\mathrm{p} = \mathbf{v} - \frac{\mathbf{v} \cdot \mathbf{n}}{\|\mathbf{n}\|^2} \cdot \mathbf{n} \tag{5}$$

, where $\vec{v}$ is the segment's frame axis and the $\vec{n}$ is the plane normal vector [24].

The rotation matrices are applied to compute the projected vectors, where the rotation matrices calculated in Madgwicks filter are in x-, y- and z-vectors. When applying the z-vector, the vector is projected on the XY plane (shown in figure 10). The outcome of the projected vector is the projected z-vector expressed in x- and y-coordinates. The frame definitions are used for the head orientation in figure 5, described in section 3.4.

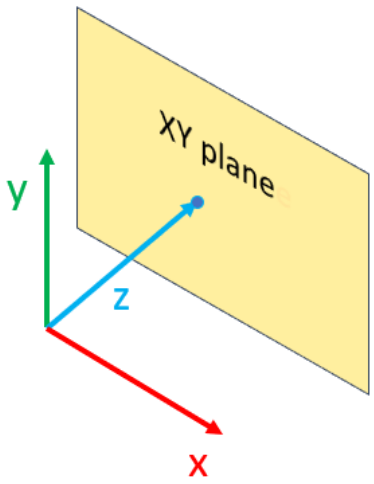

Figure 10: *Visualization of the z-vector projected on the XY-plane. As a result, the projected z-vector is expressed in x- and y-coordinates.*

4.6.2 Head Pose Sectorization

Two axes of rotation of the head (x and y) (already shown in section 3.4 figure 5) are implemented in the sector division since these are relevant to the medical case. The projected z-vectors of the IMU orientation make it possible to divide these rotation axes' movements in sectors in a circular plot.

Division of the sectors is based on the length of the projected z-vector, this by applying Pythagoras' theorem. Besides that, the division is also based on the amount of degree the projected vector deviates from the x- or y-axis. Thus to be clear, the sector plot is based on length and deviation of the x- or y-axis of the projected vector.

Since the division of the sectors is clear, the axes and multiple rings can be defined. Firstly, the x- and y-axes of the plot are based on the combination of the length and the relative deviation concerning these axes.

For example, a 90-degree pure x-rotation results in activity in one of the sectors near the x-axis, dependent on a positive or negative rotation. Furthermore, when the ”normal” z-vector its z-coordinates are negative, there is activity in the outer ring. Translating this to the case, the patient is looking downwards (in the negative z area). In figure 11, a sector plot is shown with its defined axes. Important to keep in mind is that the start position is the patient lying down in a supine position and looking up. If the head is oriented at a 90°angle concerning the x-rotated axis, the patient is behaving face forward, like the situation normally is when walking on the street.

The boundaries between what rotations in degrees are acceptable for determining are not defined, since this is part of what is yet to be researched in the whole full project. This is not within the scope of this research. The division of sectors is defined as variable which means that the division can be changed on what is desired.

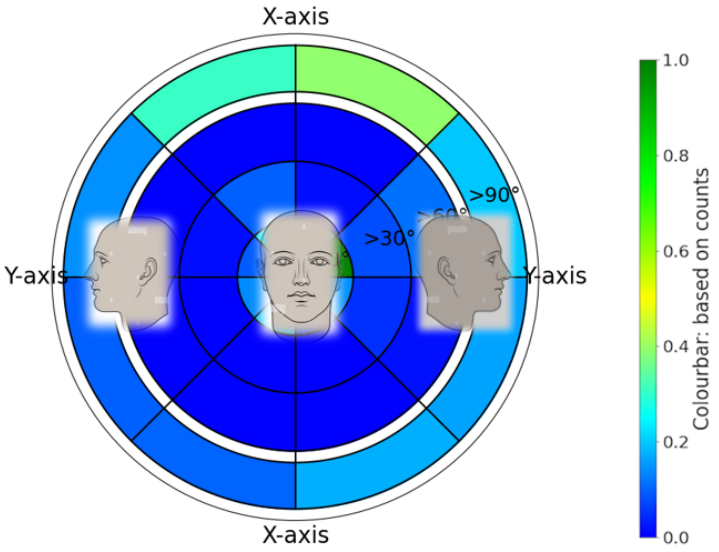

Figure 11: *Example of a circle plot where sectors are defined here respectively from centre to lateral in ranges of 0-30 °, 30-60 °, 60-90 °and > 90 °. The small white ring separates the below and greater than 90 °rings. The intensity of the head positions over time is shown with a colour scale in a range of blue to green. Blue means less occupation in the specific sector compared to the maximum and green means a high occupation. The different head poses illustrated in the figure provide an idea of head poses in those situations, based on the rotation axes in figure 5.*

5 Results

5.1 Parameter optimization

Optimising the adjustable parameter, β has been performed by calculating the RMSE over stationary periods for each β in a range of $\beta = 0.01 - 0.5$, over 50 steps.

5.1.1 RMSE vs Beta

In figure 12, β is plotted against the RMSE. The movement type here is a yaw-rotation 180-degree experiment (including small, medium and fast movement). Remarkable is the difference between slow and medium compared to the fast movement. The slow and medium movements show low RMSE values at a relatively low β,

whereas the fast movement shows low RMSE values at the higher β. In table 3, there is an overview of the best and the worst beta per movement type. The best and worst are in the graph indicated with dotted lines.

For the slow and medium movement, the same pattern is observed. Interestingly, there is a decrease of RMSE after $\beta = 0.40$ at the slow and medium movement. Contrary to the slow and medium movement the fast movement is decreasing over an increasing β.

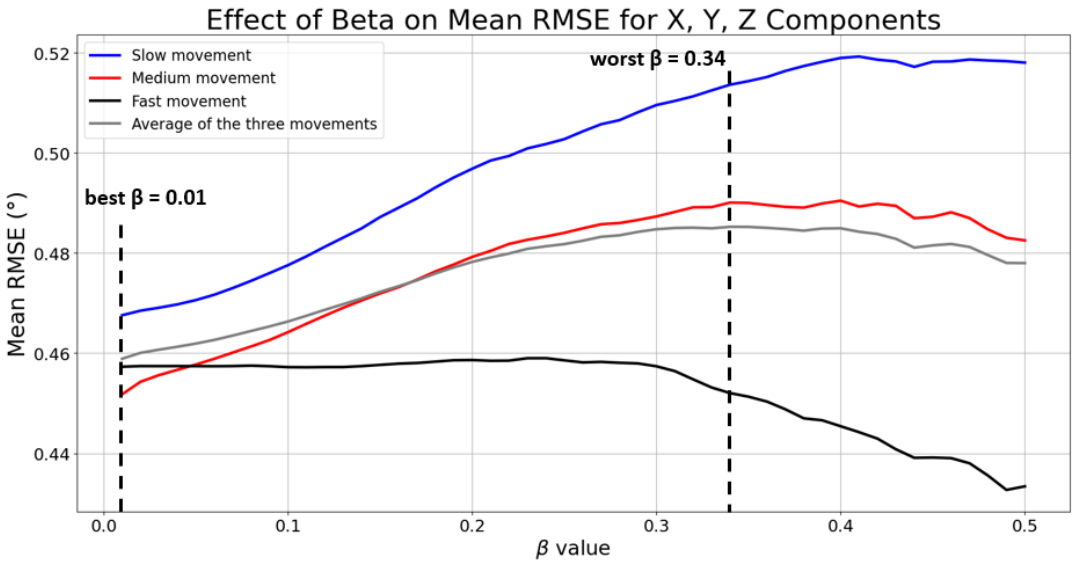

Figure 12: *RMSE at the stationary periods calculated of the z-rotation, following the β optimization method. β varies from 0.01 till 0.5. From table 3, the average best ($\beta = 0.01$) and worst ($\beta = 0.34$) parameter values are indicated as the two dotted lines.*

	Slow	Medium	Fast	Average
Best	$\beta = 0.01$	$\beta = 0.01$	$\beta = 0.49$	$\beta = 0.01$
Worst	$\beta = 0.41$	$\beta = 0.40$	$\beta = 0.24$	$\beta = 0.34$

Table 3: *Overview of the best and worst β value of the three movement types. When combining the best β per movement type, results to an overall best value of β = 0.01. This is the result when taking the mean RMSE of the three different movements.*

5.1.2 RMSE over Time

In the stationary periods, a linear increase in degrees over time is happening where the angle is expected to be 0 degrees. To show this, the RMSE of the default $\beta = 0.045$ is used and plotted against time in figure 13. The time is based on the mid-times per period, so when ten periods are selected then also ten mid-times are used from the periods. Mid-times means the time corresponding to the centre of the stationary period. A linear increase of the mean RMSE over time for all the three different type of movements is indeed observed in figure 13.

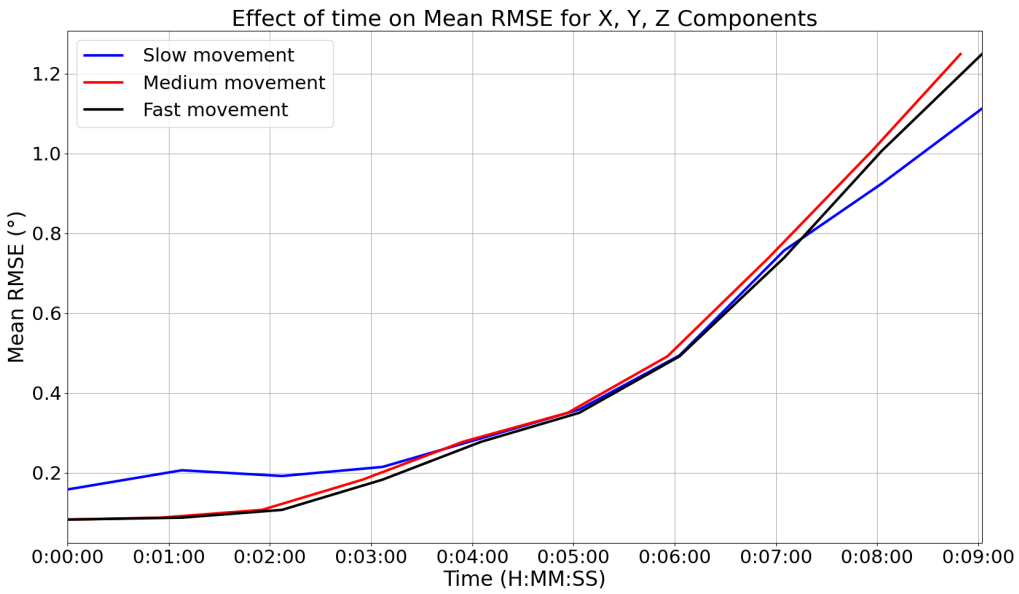

Figure 13: *Graph of the RMSE of the slow, medium and fast movement of the yaw rotation.* $\beta = 0.045$ *(default value) versus time is plotted. The 10-minutes experiment is used here. Since the RMSE is based on period selection (stationary periods), midtimes are used.*

5.2 Head Pose Sectors

The sector plots are applied to 24-hours data of two patients (indicated as ”Patient 1” and ”Patient 2”) to investigate the most occupied head poses over time. Thereby, corresponding Euler angles (X and Y) of the 24-hours data per patient are shown as reference.

Firstly, Patient 1 (figure 14). Regarding patient 1, significant activity concentrated in the third quadrant, particularly noticeable in the inner ring, below 30 degrees. In practice, this means the patient’s head is oriented within the supine looking-up range, combined with looking forward. Comparing Euler angles with the sector plot, especially focusing on the activity at the axes. Both Euler angles are behaving often in negative angles, which translates to the third quadrant, thus it corresponds with the sector plot.

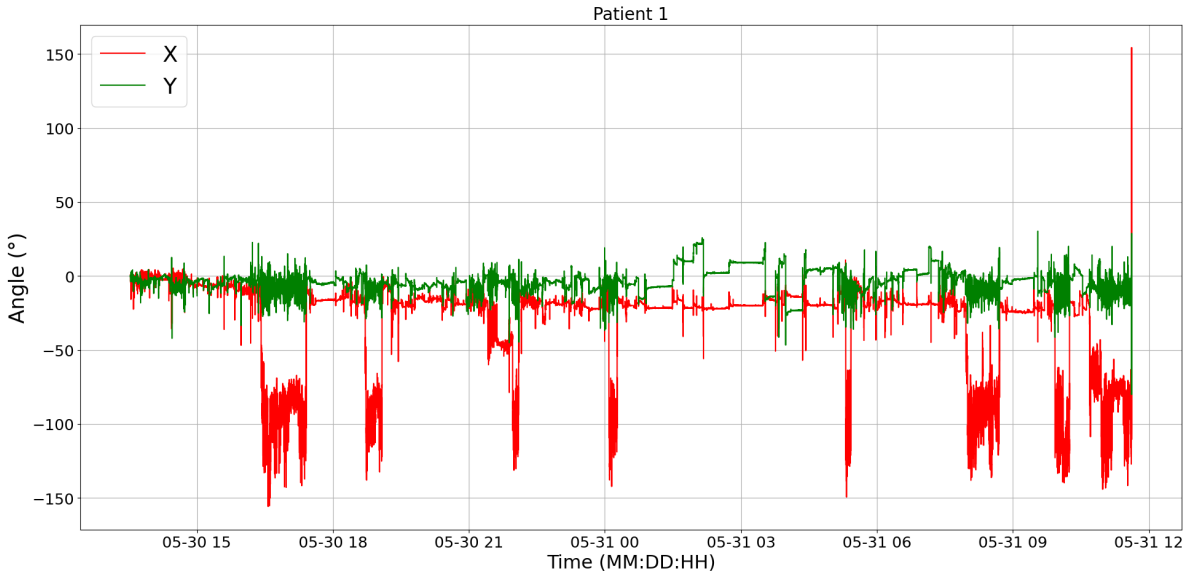

(a) Euler angle representation Patient 1

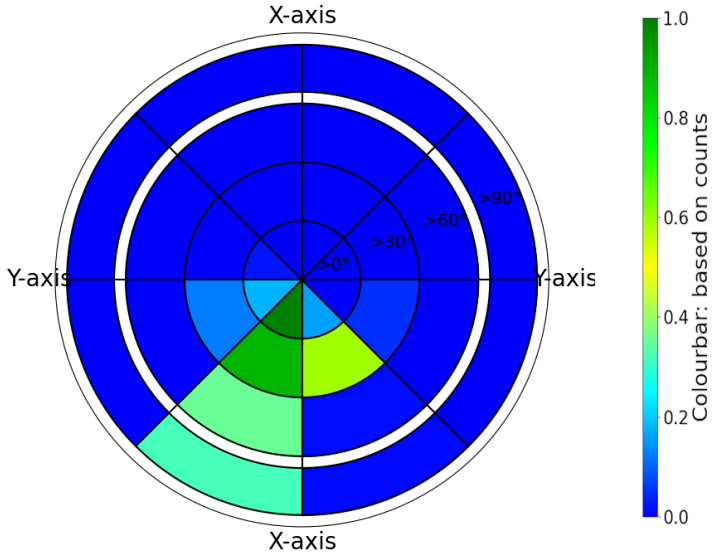

(b) Patient 1 Sector plot

Figure 14: *Euler angle representation (a) of the X and Y rotation axes of the 24-hours data of Patient 1. Sector plot visualization (b), containing the positions of the projected z-vector at the XY-plane.*

For Patient 2 (figure 15) it is notable that her head shows activity predominantly within the 90 °region of the third quadrant. The interpretation of this behaviour is that the patient's head is in an upward and rightward position most of the time. Furthermore, Patient 2 has relatively more activity in several sectors compared to Patient 1. The Euler angles correspond to this, with more activity observed at larger angles.

(a) Euler angle representation Patient 2

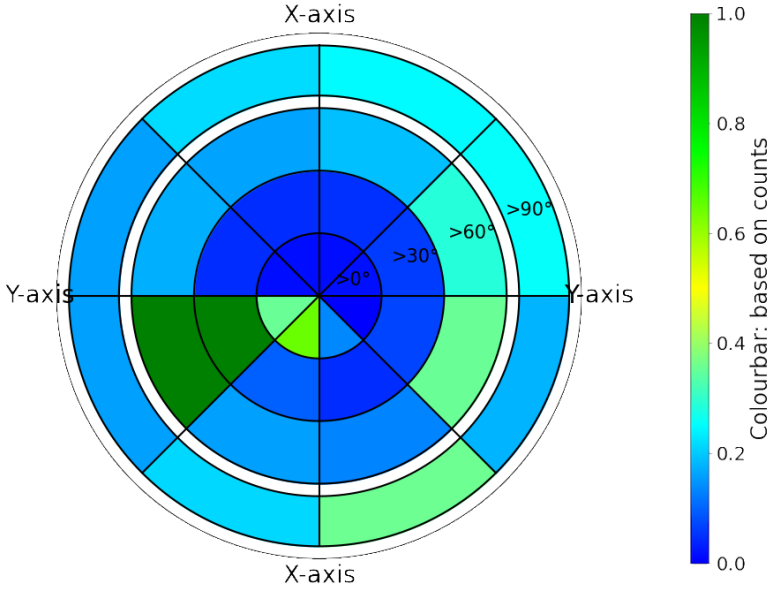

(b) Patient 2 Sector plot

Figure 15: *Euler angle representation (a) of the X and Y rotation axes of the 24-hours data of Patient 2. Sector plot visualization (b), containing the positions of the projected z-vector at the XY-plane.*

In table 4, an overview containing percentages per ring is shown. Remarkable is the difference between the behaviours of Patient 1 and Patient 2 in these percentages and rings. Patient 1's head behaved more in the first ring (36.7 %) compared to Patient 2 (17.5 %).

Circle ranges (°)	Patient 1 percentages (%)	Patient 2 percentages (%)
First ring ($0° - 30°$)	36.7 %	17.5 %
Second ring ($30° - 60°$)	44.6 %	20.6 %
Third ring ($60° - 90°$)	9.8 %	35.8 %
Negative ring ($> 90°$)	8.9 %	26.1 %

Table 4: *Percentages of head pose occupation of the 24-hours data of Patient 1 and 2, divided into first, second, third and negative ring expressed in °.*

6 Discussion

6.1 Beta Parameter Optimization

6.1.1 Expectations versus Outcomes

Based on the literature, expectations are made of how the RMSE should behave under the influence of β. Firstly at the slow movements, a low β is expected to give less RMSE, since the gyroscope is dominant in slow movements. A low β gain prioritizes the gyroscope's stability and accuracy while the accelerometers' influence on noise and biases is minimized. Since the RMSE is calculated at stationary periods, conversion from slow movement to stationary still relies on the gyroscope, which means a low β gain would give more accuracy.

For fast movement conversion to stationary periods, a higher β gain is expected to be more appropriate when focusing on accuracy. The accelerometer data can account for these quick changes in movement, which means a high beta value is more suitable for a movement with higher velocity as well for the change from a high-speed movement to a stationary period [25].

The outcomes are what is expected when looking at figure 12 in section 5.1.1. For slow motion, a low $\beta = 0.01$ results in a low RMSE and for fast motion, a relatively high $\beta = 0.49$ results in a lower RMSE. Taking the average of the RMSEs of the three different types of motion, β = 0.01 is the best value to optimise.

The movements performed are, however, not sufficient to be similar to head movements. The head movements also deal with accelerations during movement and compared to the head movements, these measurements are performed with constant velocities. Furthermore, the velocities quantified in the beta optimization experiment are maybe not representative for head movements. The ratio is in head motions not equal to each other, regarding the different velocities. Based on these results a conclusion cannot be made for an optimized β value. The observed trend suggests that the optimal β value likely resides in the lower range (around the default β = 0.045) because each of the movements performed do have a relatively low RMSE compared with the higher β region.

6.1.2 Stationary Periods

There are however some things to say about calculating the RMSE over the stationary periods. Is there a difference between the conversion of a high velocity to a stationary period and the conversion of a low velocity to a stationary period? And does the β parameter influence this conversion? To prove this, more measurements need to take place. The RMSE method used is only valuable when analyzing the stationary periods, because then there is a reference value available. When applying the RMSE to a movement it needs to be sure that the movement is constant, then the RMSE can be calculated also on these movement periods.

6.1.3 Linear Drift

Linear drift occurs over time when plotting the RMSE of the stationary periods over time. This is probably due to gyroscope drift, which is common when using an IMU and can be solved by drift compensation. In this part of the research, however, drift compensation is not applied. This means that in the conclusion assumed is that the gyro drift ”is solved”. In further research, the gyroscope drift must be compensated to obtain a valid orientation. Gyroscope drift can probably be solved by estimating the biases and compensating them [10].

6.2 Head Poses

There are a few things to consider before drawing conclusions from the head pose sectors. Firstly, positions are analyzed and not movements or accelerations over time, whereas these two are also important to get information from.

Furthermore, the outcomes of figure 14 and 15 in section 5.2 are that both Patient 1 and Patient 2 are behaving most of the time in the third quadrant. The sector plots and Euler angles correspond with each other. This behaviour seems realistic since the patient is moving generally in the third and fourth quadrants, which are more ”natural” head movements. This similar behaviour for both patients can, however, also be caused by linear drift. This linear drift is indicated in the beta optimization experiment, which means that the outcome of the sector plot is not supposed to be relied upon. Further research on the drift is recommended.

Therefore, when comparing the patient’s head behaviour in the 24-hour measurements with the assumption there is no linear drift occuring. The outcome of table 4 is that Patient 1 behaved more in the centre compared to Patient 2. Translated to the medical case, this means that Patient 1 followed the instructions better in looking up in a supine position than Patient 2.

7 Conclusion

In conclusion, regarding the main research question. the orientation of the head is estimated using the Madgwick filter. A visualization of the behaviour of the head over time is conducted and can be used in further research. Thereby, experiments such as optimization are performed and regarding these experiments, conclusions are made. These contain delving into optimizing the filter parameter β and obtaining head pose positions using a sector circular plot.

First of all, optimization of the adjustable parameter β has been performed. Through experimentation, an optimal value of β = 0.01 was identified. However, it is crucial to acknowledge that these experiments were conducted during stationary periods, whereas head movements contain varying velocities. Thus, further investigation into these dynamic movements is of importance for refining the filter optimization.

Secondly, head pose sectors are defined and applied to the 24-hours patient data. Regarding head orientation, orientations and head pose sectors are successfully obtained. Analysis of patient data revealed both patients behaved most of the time in the negative quadrants. However, as drift is indicated in the estimates regarding β optimization, the sector plots' results should not be relied upon. Thus, further research on this drift is needed. Therefore first groundwork towards a clinically useful interpretation has been made. This observation emphasizes the findings' significance and potential implications for understanding and monitoring the patient's behaviour.

8 Acknowledgements

First, I want to thank everybody at the Biomedical Signals and Systems Department for making me feel welcome. Thereby I am thankful for being able to make use of the Office Garden to work on the Thesis.

Furthermore, I want to thank dr. ir. Bert-Jan van Beijnum for being my main supervisor and chair, especially for giving feedback and good advices on my assignment.

Thereby I want to thank Msc. Sigert Mevissen, for being my daily supervisor and helping me out and being available when needed.

I want to thank my external supervisor dr. ir. Mohamed Irfan Refai for giving feedback on my assignment.

At last, I want to thank Deventer Ziekenhuis, especially dr. Marjolein Bartels for inviting me to the operating room, where I was able to attend a DMEK surgery.

9 References

References

1. Yang J. Netherlands: number of cornea transplants 2014-2018 — Statista. 2023. Available from: https://www.statista.com/statistics/1012765/number-of-cornea-transplants-in-the-netherlands/
2. Lu P, Li L, Mukaida N, and Zhang X. Alkali-induced corneal neovascularization is independent of CXCR2-mediated neutrophil infiltration. Cornea 2007; 26:199–206. DOI: 10.1097/01.ICO.0000248385.16896.34. Available from: https://journals.lww.com/corneajrnl/fulltext/2006/09000/descemet_membrane_endothelial_keratoplasty__dmek_.27.aspx
3. Donaghy C, Vislisel J, and Greiner M. Descemet Membrane Endothelial Keratoplasty (DMEK). 2015. Available from: https://webeye.ophth.uiowa.edu/eyeforum/tutorials/cornea-transplant-intro/5-DMEK.htm
4. Cornea Research Foundation of America - Descemet's Stripping Only (DSO). Available from: https://www.cornea.org/Learning-Center/Descemet-s-Stripping-Only-%28DSO%29.aspx
5. Quaternions for Orientation. Available from: https://blog.endaq.com/quaternions-for-orientation
6. Madgwick SOH. An efficient orientation filter for inertial and inertial/magnetic sensor arrays. 2010. Available from: https://ahrs.readthedocs.io/en/latest/filters/madgwick.html
7. Madgwick S, Harrison A, and Vaidyanathan R. Estimation of IMU and MARG orientation using a gradient descent algorithm ACT Profile Report: State. Graduating Class 2012. Montana. IEEE International Conference on Rehabilitation Robotics Rehab Week Zurich, ETH Zurich Science City, Switzerland, 2011 :1–7. Available from: http://proxying.lib.ncsu.edu/index.php?url=http://search.ebscohost.com/login.aspx?direct=true&db=eric&AN=ED535043&site=ehost-live&scope=site
8. Ludwig SA. Optimization of Control Parameter for Filter Algorithms for Attitude and Heading Reference Systems. *2018 IEEE Congress on Evolutionary Computation (CEC)*. IEEE, 2018 Jul :1–8. DOI: 10.1109/CEC.2018.8477725. Available from: https://ieeexplore.ieee.org/document/8477725/
9. Wilson S, Eberle H, Hayashi Y, Madgwick SO, McGregor A, Jing X, and Vaidyanathan R. Formulation of a new gradient descent MARG orientation algorithm: Case study on robot teleoperation. Mechanical Systems and Signal Processing 2019 Sep; 130:183–200. DOI: 10.1016/J.YMSSP.2019.04.064
10. Caruso M, Gastaldi L, Pastorelli S, Cereatti A, and Digo E. An ISB-consistent Denavit-Hartenberg model of the human upper limb for joint kinematics optimization: validation on synthetic and robot data during a typical rehabilitation gesture. *2022 44th Annual International Conference of the IEEE Engineering in Medicine & Biology Society (EMBC)*. IEEE, 2022 Jul :1805–8. DOI: 10.1109/EMBC48229.2022.9871201. Available from: https://ieeexplore.ieee.org/document/9871201/
11. Shiavi R. Introduction to Applied Statistical Signal Analysis. Elsevier, 2007. Chap. 5. DOI: 10.1016/B978-0-12-088581-7.X5015-8. Available from: https://linkinghub.elsevier.com/retrieve/pii/B9780120885817X50158

12. Caraballo L. Quaternion Rotation: A Magical Journey to the Fourth Dimension MA 398: Senior Seminar. Available from: https://digitalcommons.sacredheart.edu/acadfest/2022/all/165

13. Rotation matrix. Available from: http://en.wikipedia.org/wiki/Rotation_matrix

14. Lecture L29-3D Rigid Body Dynamics 3D Rigid Body Dynamics: Euler Angles

15. Article Detail. Available from: https://base.movella.com/s/article/Understanding-Gimbal-Lock-and-how-to-prevent-it?language=en_US

16. Bloßfeld M, Zeitlhöfler J, Rudenko S, and Dettmering D. Observation-based attitude realization for accurate jason satellite orbits and its impact on geodetic and altimetry results. Remote Sensing 2020 Feb; 12. DOI: 10.3390/RS12040682. Available from: https://www.researchgate.net/figure/llustrates-the-principle-of-gimbal-lock-The-outer-blue-frame-represents-the-x-axis-the_fig4_338835648

17. Wang C, Guo Y, and Song X. Head Pose Estimation via Manifold Learning. *Manifolds - Current Research Areas*. InTech, 2017 Jan. DOI: 10.5772/65903. Available from: http://www.intechopen.com/books/manifolds-current-research-areas/head-pose-estimation-via-manifold-learning

18. Danisman T and Bilasco IM. In-plane face orientation estimation in still images. Multimedia Tools and Applications 2016 Jul; 75:7799–829. DOI: 10.1007/s11042-015-2699-x. Available from: http://link.springer.com/10.1007/s11042-015-2699-x

19. Arcoverde Neto EN, Duarte RM, Barreto RM, Magalhães JP, Bastos CC, Ren TI, and Cavalcanti GD. Enhanced real-time head pose estimation system for mobile device. Integrated Computer-Aided Engineering 2014 Apr; 21:281–93. DOI: 10.3233/ICA-140462. Available from: https://www.medra.org/servlet/aliasResolver?alias=iospress&doi=10.3233/ICA-140462

20. Jackson D. Open Movement. 2019. Available from: https://github.com/digitalinteraction/openmovement

21. Seel T, Raisch J, and Schauer T. IMU-based joint angle measurement for gait analysis. Sensors (Switzerland) 2014 Apr; 14:6891–909. DOI: 10.3390/S140406891. Available from: www.mdpi.com/journal/sensorsArticle

22. Christie D and Neill SP. Measuring and Observing the Ocean Renewable Energy Resource. *Comprehensive Renewable Energy*. 2022nd ed. Elsevier, 2022 :149–75. DOI: 10.1016/B978-0-12-819727-1.00083-2. Available from: https://linkinghub.elsevier.com/retrieve/pii/B9780128197271000832

23. Cho YS, Jang SH, Cho JS, Kim MJ, Lee HD, Lee SY, and Moon SB. Evaluation of Validity and Reliability of Inertial Measurement Unit-Based Gait Analysis Systems. Annals of Rehabilitation Medicine 2018 Dec; 42:872–83. DOI: 10.5535/arm.2018.42.6.872. Available from: http://www.e-arm.org/journal/view.php?doi=10.5535/arm.2018.42.6.872

24. Bhagubai MMC, Wolterink G, Schwarz A, Held JPO, Van Beijnum BJF, and Veltink PH. Quantifying Pathological Synergies in the Upper Extremity of Stroke Subjects With the Use of Inertial Measurement Units: A Pilot Study. IEEE Journal of Translational Engineering in Health and Medicine 2021; 9:1–11. DOI: 10.1109/JTEHM.2020.3042931. Available from: https://ieeexplore.ieee.org/document/9284460/

25. Chen H, Schall MC, and Fethke NB. Gyroscope vector magnitude: A proposed method for measuring angular velocities. Applied Ergonomics 2023 May; 109:103981. DOI: 10.1016/J.APERGO.2023.103981

10 List of symbols

Table 5: *List of symbols.*

Symbols	Meaning and unit
$DMEK$	Descemet's Membrane Endothelial Keratoplasty
IMU	Inertial Measurement Unit
$AHRS$	Attitude and Heading Reference System
DOF	Degrees of Freedom
Hz	Hertz
dps	degrees per second
g	standard gravity
GME	Gyroscope Measurement Error
IDE	Integrated Development Environment
$RMSE$	Root Mean Square Error

A Appendix

A.1

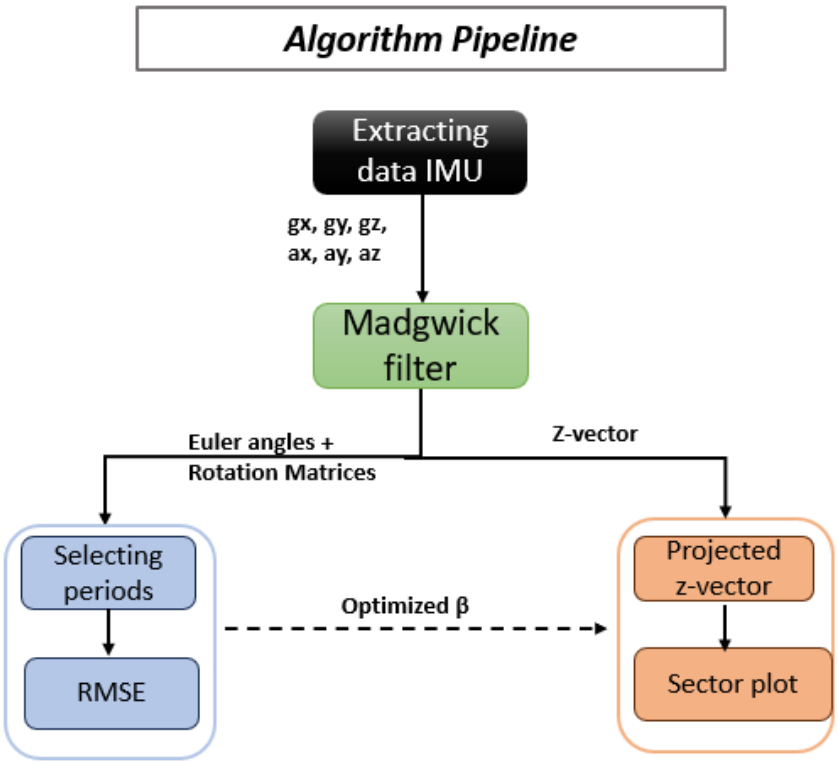

Figure 16: *Algorithm pipeline, consisting the steps made to achieve the desired output. RMSE is applied to Madgwick's algorithm data to achieve the β optimization and the z-vector of Madgwick's algorithm is used to calculate the projected z-vector to acquire the sector plots.*